Molecular Crystals and Liquid Crystals

ISSN: 1542-1406 (Print) 1563-5287 (Online) Journal homepage: http://www.tandfonline.com/loi/gmcl20

Synthesis, Molecular Structure, Spectral, Thermal, and DFT Studies of an Organic Crystal: 1-(benzo[d][1,3]dioxol-5-yl)-3-phenylprop-2-en-1-One

S. Senthan, S. Srinivasan & S. Kabilan

To cite this article: S. Senthan, S. Srinivasan & S. Kabilan (2015) Synthesis, Molecular Structure, Spectral, Thermal, and DFT Studies of an Organic Crystal: 1-(benzo[d][1,3]dioxol-5-yl)-3-phenylprop-2-en-1-One, Molecular Crystals and Liquid Crystals, 609:1, 249-265, DOI: 10.1080/15421406.2014.963210

To link to this article: http://dx.doi.org/10.1080/15421406.2014.963210

Published online: 11 Apr 2015.

Mol. Cryst. Liq. Cryst., Vol. 609: pp. 249–265, 2015

ISSN: 1542-1406 print/1563-5287 online
DOI: 10.1080/15421406.2014.963210

Synthesis, Molecular Structure, Spectral, Thermal, and DFT Studies of an Organic Crystal: 1-(benzo[d][1,3]dioxol-5-yl)-3-phenylprop-2-en-1-One

S. SENTHAN,[1] S. SRINIVASAN,[2] AND S. KABILAN[1,*]

[1]Department of Chemistry, Annamalai University, Annamalainagar, Tamilnadu, India
[2]Department of Chemistry (DDE Wing), Annamalai University, Annamalainagar, Tamilnadu, India

The synthesis, characterization, thermal stability, optical spectroscopic, FT-IR, and theoretical studies of a novel 1-(benzo[d][1,3]dioxol-5-yl)-3-phenylprop-2-en-1-one (BDP) is reported. Structure is elucidated by single-crystal X-ray diffraction analysis. The crystal belongs to monoclinic system with centrosymmetric space group $P2_1/c$ *with four molecules in the unit cell. The various mode of vibration present in the molecule are confirmed by FT-IR analysis and the experimental pattern is compared with theoretical one. The crystal is transparent in the entire visible region having a lower optical cut-off ∼390 nm and the observed values are compared with theoretical values. The surface morphology of the specimen was analyzed by scanning electron microscopy (SEM). The TG/DTA study reveals the purity of the materials and no decomposition is observed up to the melting point. Theoretical calculations were performed to derive the optimized geometry, average polarizability (α), dipole moment (μ), first-order molecular hyperpolarizability (β), HOMO–LUMO, chemical hardness (η), softness (S), and electronegativity (χ) by using B3LYP/6-31G(d,p) level of theory. The atomic charge distributions of the various atoms present in BDP are obtained by Mulliken charge population analysis.*

Keywords Crystal structure; HOMO–LUMO; hyperpolarizability; thermal analysis; vibrational spectroscopy

1. Introduction

Chalcones belonging to flavonoid family are the biosynthetic product of shikimate pathway. Chalcones and its derivatives have drawn a greater attention due to their potent broad spectrum pharmacological applications. They are the key precursors in the synthesis of many of

*Address correspondence to Dr. S. Kabilan, Department of Chemistry, Annamalai University, Annamalainagar 608 002, Tamilnadu, India. E-mail: kabilan.s.1600@annamalaiuniversity.ac.in

Color versions of one or more of the figures in the article can be found online at www.tandfonline.com/gmcl.

the biologically important hetero cycles such as pyrazolines, pyrimidines, flavones etc. Chalcones and their derivatives are easily available, not only by isolation from natural products but also by the methods of classical and combinatorial synthesis. The cytotoxic, anticancer, chemopreventative and mutagenic properties of a number of chalcones have been reviewed [1, 2]. The antibacterial, fungistatic, and fungicidal properties of these compounds have been reviewed and their analogs are used as potential therapeutic agents in diseases of the cardiovascular system [3]. Heterocyclic analogs of chalcons exhibit anti-inflammatory, antitumour [4–6], antibacterial, antifungal [7], antitubercular, antiviral, antiprotozal, and gastroprotective activities. In addition, with appropriate substituents, chalcones are a class of nonlinear optical materials [8–17]. Among the many known organic nonlinear optical materials, chalcones exhibit extremely high and fast nonlinearity [18–21] and its derivatives have excellent blue light transmittance and good crystallizability [22, 23]. Higher the charge transfer, larger is the hyperpolarizability (β). These types of materials are chosen since they are very promising class due to large beta values and the possibility of enhancing nonlinearity by molecular design. In the present investigation, we report the synthesize and characterization of 1-(benzo[d][1,3]dioxol-5-yl)-3-phenylprop-2-en-1-one by X-ray diffraction, spectral (FT-IR and UV–visible), thermal, morphological, and the theoretical predictions were carried out by using B3LYP/6-31G(d, p) level of theory.

2. Experimental Details

2.1. Synthesis and Growth

BDP was synthesized by mixing stochiometric amounts of 3,4-methylenedioxy acetophenone (0.001 mol) and benzaldehyde (0.001 mol) in the molar ratio of 1:1 (Scheme 1). The reactants were dissolved in ethanol, thoroughly mixed using a magnetic stirrer (10 min) and 10% NaOH solution was added drop by drop at 30°C for 30 min. After stirring for 2 h, the contents of the flask were poured into ice-cold water. The solid precipitate formed was collected by filtration, dried and purified by recrystallization process using ethanol as a solvent (yield: 90%). The completeness of the reaction was monitored by thin layer chromatography.

Single crystals of BDP were grown from an ethanolic solution by slow evaporation solution growth technique at room temperature. A saturated solution of BDP in ethanol was prepared and the solution stirred well for 3 h at room temperature to obtain a homogenous solution. A beaker containing BDP solution was tightly covered with thin polythene sheet to control the evaporation rate of the solvent and kept undisturbed in dust free environment. Numerous tiny crystals were formed at the bottom of the container due to spontaneous nucleation. The single crystal suitable for the X-ray diffraction study was harvested in a period of 4–5 days.

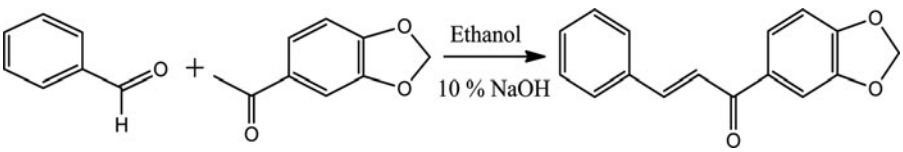

Scheme 1.

2.2. Characterization Studies

The structural analysis of BDP was carried out for a selected needle of approximately 0.35 × 0.30 × 0.30 mm^3 using a BRUKER AXS (Kappa APEXII) X-ray diffractometer. The powder XRD analysis was performed using a Philips X'pert Pro Triple axis X-ray diffractometer using a wavelength of 1.540 Å with a step size of 0.008 Å. FT-IR spectrum was recorded using an AVATAR 330 FTIR by KBr pellet technique in the range of 400–4000 cm^{-1}. Morphologies of the samples were observed on a JEOL JSM 5610 LV scanning electron microscope. A CARY−5E UV−VIS-NIR spectrophotometer was used for the UV−vis studies. Thermogravimetry and differential thermal analyses were recorded on NETZSCH STA 449F3 thermal analyzer in nitrogen atmosphere.

2.3. Computational Details

The entire calculations were performed using the *GAUSSIAN 09W* [24] program package on a personal computer without any constraints on the geometry using density functional theory (DFT) method with 6−31G(*d,p*) as the basis set [25]. By the use of the *GAUSSVIEW* 5.0 molecular visualization program [26], the optimized structure of the molecule has been visualized.

3. Results and Discussion

3.1. Molecular Structure

The structural analysis of BDP was carried out by single X–ray diffraction analysis and the crystallographic parameters are listed in Table 1. It belongs to monoclinic system with space group $P2_1/c$. The ORTEP and packing diagrams are shown in Figs 1 and 2. The optimization of BDP was carried out using B3LYP/6-31G(d,p) level of basis set and the optimized atom numbering is shown in Fig. 3. The comparative optimized structural parameters such as bond lengths and angles along with the XRD data is listed in Table 2. As seen from Table 2, most of the optimized bond lengths are slightly higher than the experimental values and the angles are slightly different from the experimental ones, because the molecular states are different during experimental and theoretical processes. The most variation in the angles at C(3)-C(2)-C(1) and C(2)-C(3)-C(4) are due to the interaction between carbonyl oxygen (C1O1) and aromatic hydrogen C5 carbon atom. The molecular structure of BDP is non-planar. Taking C4–C9 phenyl ring as plane 1, C10–C16 bicyclic ring as plane 2 and the central C1–C2 = C3 as plane 3, the dihedral angle between them, DA_{12}, DA_{13}, and DA_{23} are, 20.10°, 16.88°, and 8.55°, respectively.

3.2. FT-IR Analysis

The FT-IR spectrum of BDP (Fig. 4a) was recorded using an AVATAR 330 FTIR by KBr pellet technique in the range of 400–4000 cm^{-1}. The sharp absorption band appeared at ∼1653 cm^{-1} is due to -CO stretching of α, β-unsaturated carbonyl group. The bands appeared at ∼2903 and ∼2782 cm^{-1} are due to aliphatic C-H stretching vibrations. The aromatic C-H stretching vibration appeared at ∼3073 cm^{-1}. The strong absorption bands at ∼1589 and ∼1504 cm^{-1} are corresponding to C = C stretching vibration. The bands observed at about 982, 814, and 767 cm^{-1} is due to aromatic C-H bending vibrations.

Table 1. Crystal data and structure refinement for BDP

Identification code	shelxl
Empirical formula	$C_{16}H_{12}O_3$
Formula weight	255.76
Temperature	293(2) K
Wavelength	0.71073 Å
Crystal system, space group	Monoclinic, $P2_1/c$
Unit cell dimensions	a = 5.796(5) Å, α = 90.000(5)°. b = 8.694(5) Å, β = 91.467(5)°. c = 24.411(5) Å, γ = 90.000(5)°.
Volume	1229.7(13) $Å^3$
Z, Calculated density	4, 1.381 Mg/m^3
Absorption coefficient	0.096 mm^{-1}
$F(000)$	535
Crystal size	0.30 × 0.30 × 0.190 mm^3
Theta range for data collection	1.669 to 27.998°.
Limiting indices	−7<=h<=7, −11<=k<=11, −32<=l<=32
Reflections collected/unique	14116 / 2977 [R(int) = 0.0265]
Completeness to theta = 25.00	100.0%
Absorption correction	Semi-empirical from equivalents
Max. and min. transmission	0.9973 and 0.9534
Refinement method	Full-matrix least-squares on F^2
Data/restraints/parameters	2977/0/172
Goodness-of-fit on F^2	1.128
Final R indices [$I > 2$sigma (I)]	$R1 = 0.0415$, w$R2 = 0.1379$
R indices (all data)	$R1 = 0.0710$, w$R2 = 0.1688$
Extinction coefficient	0.039(5)
Largest diff. peak and hole	0.202 and −0.245 e.A^{-3}

BDP belongs to C1 point group symmetry and it consists of 31 atoms which undergoes 87 normal modes of vibrations. Theoretical FT-IR spectrum of BDP is shown in Fig. 4b. The observed experimental and theoretical FT–IR vibrational bands of BDP are listed in Table 3.

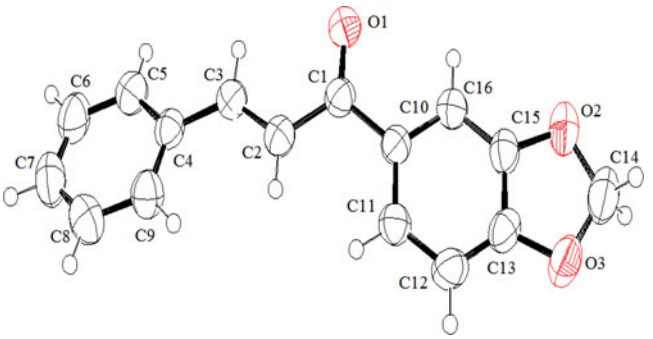

Figure 1. ORTEP diagram of BDP.

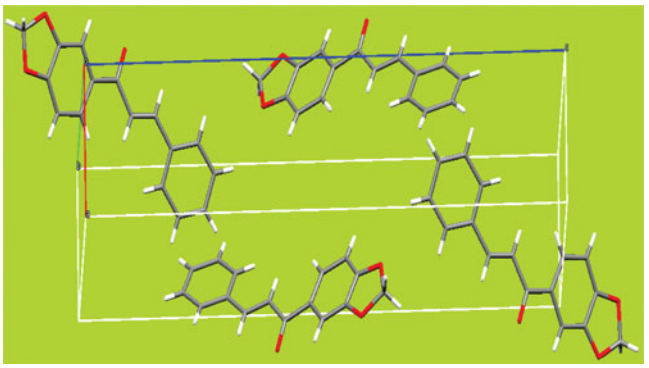

Figure 2. Packing diagram of BDP.

3.3. Powder XRD

The indexed powder XRD pattern of as-grown BDP is shown in Fig. 5. The XRD profiles show that a sample is of single phase without detectable impurity. The well defined Bragg's peaks at specific 2θ angles show high crystallinity of the material.

3.4. SEM

The SEM images (Fig. 6) were taken at maginification values for 2,500× and 5,000× with maximum values of 15 kV using a JEOL JSM 5610 LV scanning electron microscope. Small pores and crystal voids are observed on the surface of the BDP.

3.5. Optical Absorption Studies

UV–vis spectrum of BDP was recorded using ethanol as a solvent. The optical absorbance spectrum shows minimum absorbance in the visible region and the lower cut-off wavelength is ∼390 nm (Fig. 7a). To support experimental observations, the theoretical electronic absorbance spectrum of BDP has been carried out (Fig. 7b). On the basis of a fully optimized ground state structure, the electronic spectrum of BDP was computed in ethanol

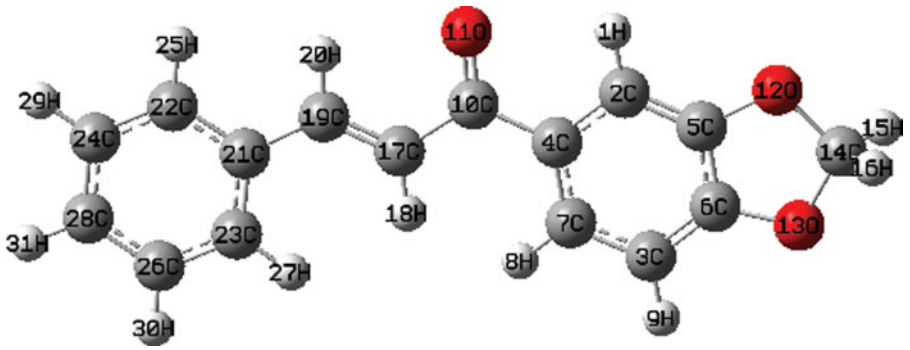

Figure 3. Optimized molecular structure of BDP.

Table 2. The calculated geometrical parameters of BDP

Parameters	XRD data	Theoretical data
Bond length (Å)		
O(1)-C(1)	1.2227 (19)	1.232
C(1)-C(2)	1.470 (2)	1.478
C(1)-C(10)	1.482 (2)	1.501
O(2)-C(15)	1.3759 (19)	1.375
O(2)-C(14)	1.411 (2)	1.429
C(2)-C(3)	1.317 (2)	1.358
C(2)-H(2)	0.93	1.085
C(4)-C(9)	1.381 (2)	1.412
C(4)-C(5)	1.383 (2)	1.410
C(4)-C(3)	1.461 (2)	1.464
O(3)-C(13)	1.3638 (18)	1.367
O(3)-C(14)	1.426 (3)	1.437
C(3)-H(3)	0.93	1.090
C(5)-C(6)	1.374 (2)	1.392
C(5)-H(5)	0.93	1.081
C(6)-C(7)	1.363 (3)	1.396
C(6)-H(6)	0.93	1.086
C(7)-C(8)	1.373 (3)	1.396
C(7)-H(7)	0.93	1.086
C(8)-C(9)	1.380 (2)	1.390
C(8)-H(8)	0.93	1.086
C(9)-H(9)	0.93	1.087
C(10)-C(11)	1.383 (2)	1.402
C(10)-C(16)	1.404 (2)	1.417
C(11)-C(12)	1.385 (2)	1.403
C(11)-H(11)	0.93	1.083
C(12)-C(13)	1.356 (2)	1.381
C(12)-H(12)	0.93	1.083
C(14)-H(14A)	0.97	1.094
C(14)-H(14B)	0.97	1.098
C(15)-C(16)	1.350 (2)	1.373
C(15)-C(13)	1.368 (2)	1.396
C(16)-H(16)	0.93	1.082
Bond angle (°)		
O(1)-C(1)-C(2)	120.58 (14)	123.81
O(1)-C(1)-C(10)	119.58 (13)	118.72
Bond angle (°)		
C(2)-C(1)-C(10)	119.82 (13)	117.43
C(15)-O(2)-C(14)	105.92 (15)	106.09
C(3)-C(2)-C(1)	121.10 (14)	131.62
C(3)-C(2)-H(2)	119.5	114.29
C(1)-C(2)-H(2)	119.5	114.08
C(9)-C(4)-C(5)	118.34 (14)	117.99
C(9)-C(4)-C(3)	122.44 (14)	125.08

(*Continued on next page*)

Table 2. The calculated geometrical parameters of BDP (*Continued*)

Parameters	XRD data	Theoretical data
C(5)-C(4)-C(3)	119.22 (14)	116.02
C(13)-O(3)-C(14)	105.79 (13)	105.98
C(2)-C(3)-C(4)	127.64 (15)	136.22
C(2)-C(3)-H(3)	116.2	112.63
C(4)-C(3)-H(3)	116.2	111.09
C(6)-C(5)-C(4)	121.12 (17)	120.29
C(6)-C(5)-H(5)	119.4	120.84
C(4)-C(5)-H(5)	119.4	118.85
C(7)-C(6)-C(5)	119.97 (17)	120.87
C(7)-C(6)-H(6)	120	119.87
C(5)-C(6)-H(6)	120	119.24
C(6)-C(7)-C(8)	119.94 (16)	119.60
C(6)-C(7)-H(7)	120	120.24
C(8)-C(7)-H(7)	120	120.14
C(7)-C(8)-C(9)	120.27 (17)	119.75
C(7)-C(8)-H(8)	119.9	120.31
C(9)-C(8)-H(8)	119.9	119.92
C(8)-C(9)-C(4)	120.33 (16)	121.46
C(8)-C(9)-H(9)	119.8	119.44
C(4)-C(9)-H(9)	119.8	119.08
C(11)-C(10)-C(16)	119.67 (13)	120.04
C(11)-C(10)-C(1)	122.99 (13)	123.34
C(16)-C(10)-C(1)	117.34 (13)	116.56
C(10)-C(11)-C(12)	121.67 (14)	121.89
C(10)-C(11)-H(11)	119.2	119.98
C(12)-C(11)-H(11)	119.2	118.08
Bond angle (°)		
C(13)-C(12)-C(11)	117.20 (15)	116.78
C(13)-C(12)-H(12)	121.4	121.38
C(11)-C(12)-H(12)	121.4	121.82
O(2)-C(14)-O(3)	108.42 (14)	108.01
O(2)-C(14)-H(14A)	110	109.76
O(3)-C(14)-H(14A)	110	109.21
O(2)-C(14)-H(14B)	110	109.65
O(3)-C(14)-H(14B)	110	109.26
H(14A)-C(14)-H(14B)	108.4	110.86
C(16)-C(15)-C(13)	122.51 (14)	122.09
C(16)-C(15)-O(2)	127.79 (15)	128.47
C(13)-C(15)-O(2)	109.70 (14)	109.42
C(15)-C(16)-C(10)	117.30 (14)	117.37
C(15)-C(16)-H(16)	121.4	122.83
C(10)-C(16)-H(16)	121.4	119.79
C(12)-C(13)-O(3)	128.24 (15)	128.31
C(12)-C(13)-C(15)	121.64 (14)	121.78
O(3)-C(13)-C(15)	110.12 (14)	109.89

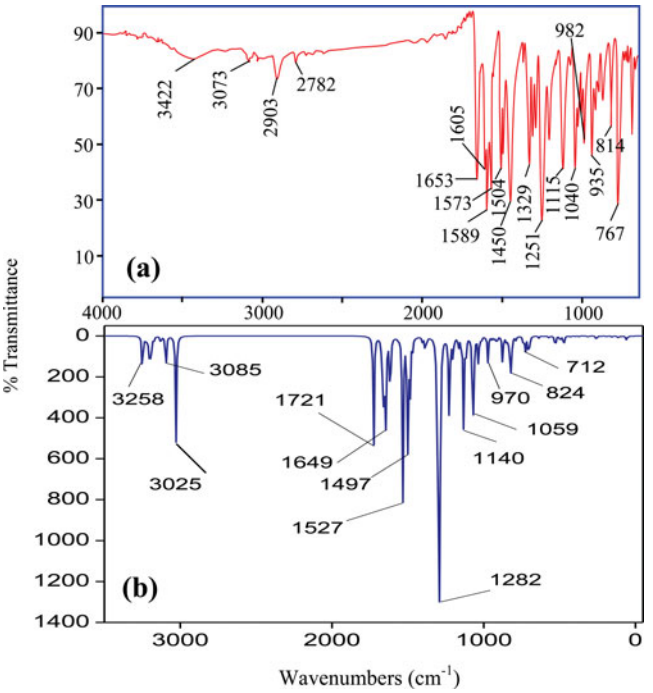

Figure 4. FT-IR spectra of BDP: (a) Experimental and (b) Theoretical.

environment using TD–DFT method and the calculated absorption peak, excitation energy, and oscillator strengths of BDP are listed in Table 4.

3.6. Thermal Analysis

In order to exam the thermal stability of BDP crystal, the thermogravimetric analysis (TG) and differential thermal analysis (DTA) have been carried out simultaneously in nitrogen atmosphere (Fig. 8). Weight loss due to melting and decomposition is observed at ∼250°C. The absence of endo or exothermic transition below 250°C indicates the absence of the other phase transitions before the melting point of BDP.

Table 3. Observed FT-IR vibrational bands of BDP (cm^{-1})

Experimental	Theoretical	Assignments of vibration
1653	1649	C=O stretching
1504	1497	aromatic C=C stretching
3073	3085	aromatic C−H stretching
2903	—	aliphatic C−H stretching
982	970	C−H bending

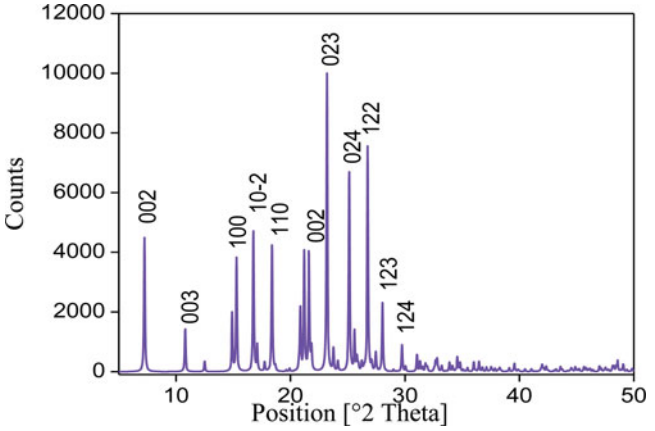

Figure 5. Powder XRD pattern of BDP.

3.7. First-Order Molecular Hyperpolarizability

The first-order molecular hyperpolarizability of BDP was calculated using B3LYP/6-31G (d, p) level of basis set, based on the finite-field approach. The first-order hyperpolarizability is a third rank tensor that can be described by a $3 \times 3 \times 3$ matrix. The 27 components of the 3D matrix can be reduced to 10 components due to Kleinman symmetry [27]. It can be given in the lower tetrahedral format. It is obvious that the lower part of the $3 \times 3 \times 3$ matrices is a tetrahedral. The components of β are defined as the coefficients in the Taylor series expansion of the energy in the external electric field. When the external electric field is weak and homogeneous, this expansion becomes:

$$E = E^{0-}\mu_\alpha F_\alpha^- 1/2\alpha_{\alpha\beta} F_\alpha F_{\bar{\beta}} 1/6\beta_{\alpha\beta\gamma} F_\alpha F_\beta F_\gamma$$

where E^0 is the energy of the unperturbed molecules, F_α is the field at the origin, and μ_α, $\alpha_{\alpha\beta}$ and $\beta_{\alpha\beta\gamma}$ is the components of the dipole moment, polarizability and the first-order molecular hyperpolarizability, respectively. The total static dipole moment (μ), the mean polarizability (α_0) and the mean first-order molecular hyperpolarizability (β_0), using the *x*,

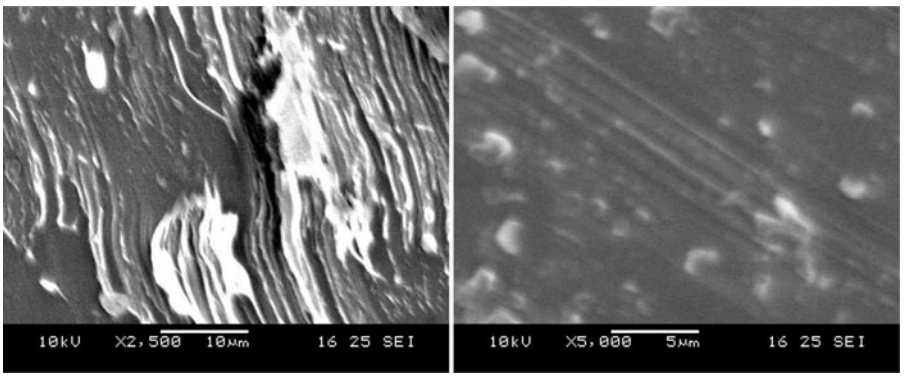

Figure 6. SEM images of BDP.

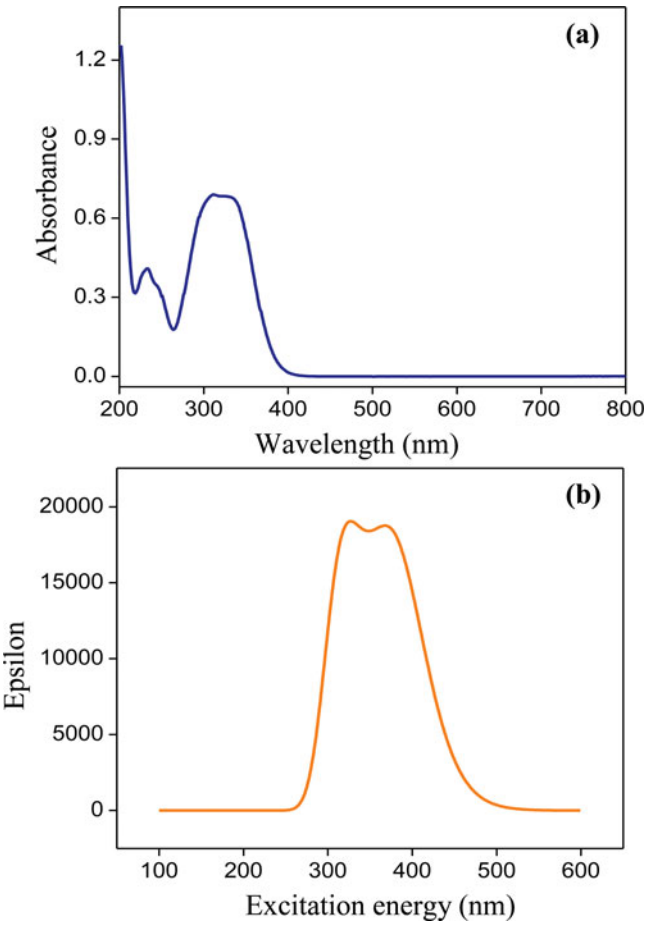

Figure 7. UV-vis spectra of BDP: (a) Experimental and (b) Theoretical.

y, z components are defined as

$$\mu = \left(\mu_x^2 + \mu_y^2 + \mu_x^2\right)^{1/2}$$
$$\alpha_0 = \left(\alpha_{xx} + \alpha_{yy} + \alpha_{zz}\right)/3$$
$$\beta_0 = \left(\beta_x^2 + \beta_y^2 + \beta_z^2\right)1/2$$

Table 4. Theoretical electronic absorption spectral values of BDP

Wavelength (λ_{max}, nm)	Excitation energies (eV)	Oscillator strengths (*f*)
380.46	3.2588(66 → 67)	0.3891
369.75	3.3532(62 → 67), (63 → 67)(64 → 67), (65 → 67), (66 → 67)	0.0243
318.92	3.8877(64 → 67), (65 → 67)	0.4205

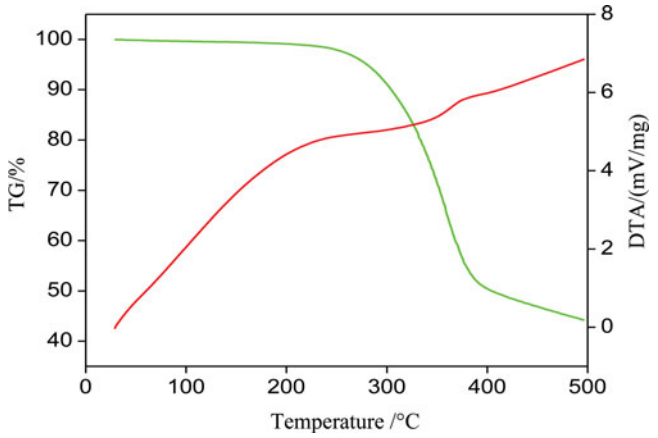

Figure 8. TG/DTA curves of BDP.

where,

$$\beta_x = \beta_{xxx} + \beta_{xyy} + \beta_{xzz}$$
$$\beta_y = \beta_{yyy} + \beta_{xxy} + \beta_{yzz}$$
$$\beta_z = \beta_{zzz} + \beta_{xxz} + \beta_{yyz}$$

Organic molecules containing conjugated π electrons are characterized by large values of molecular first-order hyperpolarizabilities and analyzed by means of vibrational spectroscopy [28–31]. The intramolecular charge transfer from the donor to acceptor group through a single-double bond conjugated path can induce large variations on both the molecular dipole moment and polarizability [32].

In present study, the calculated total molecular dipole moment (μ), polarizability (α), and mean first-order molecular hyperpolarizability of the specimen are 5.192 Debye, 29.396 esu, and 13.834 $\times$ 10^{-30} esu, respectively, and the calculated components are listed in Table 5. The total dipole moment of the BDP is $\sim$ 3.7 times greater than that of urea and first-order molecular hyperpolarizability is $\sim$37 times greater than that of urea (for urea, $\mu = 1.3732$ and $\beta = 0.3728 \times 10^{-30}$ esu obtained by HF/6-311G(d,p)). Higher β is associated with high charge transfer. Tuning the electronics properties by substitution, it could be possible to enhance the first-order molecular hyperpolarizability and engineer the nonlinearity in the macrolevel. Table 6 shows the hyperpolarizability of BDP and some chalcone derivatives reported in the literature.

3.8. Molecular Electrostatic Potential

Molecular electrostatic potential (MEP) at a point in the space around a molecule gives an indication of the net electrostatic effect produced at that point by the total charge distribution (electron + proton + nucleus) of the atom or molecule and correlates with dipole moments, electronegativity, partial charges, and chemical reactivity of the molecule. The different values of the electrostatic potential at the surface are represented by different colors: red represents regions of most negative electrostatic potential, blue represents regions of most positive electrostatic potential, and green represents regions of zero potential. The order

Table 5. The calculated β components, β_{tot} ($\times 10^{-30}$ esu), dipole moment (in D), polarizabilty (α in esu), and HOMO–LUMO (eV), electronegativity (eV), hardness (eV), and softness (eV^{-1}) values of BDP

First-order molecular hyperpolarizability	
β_{xxx}	1644.427
β_{xxy}	−126.484
β_{xyy}	−34.356
β_{yyy}	93.665
β_{xxz}	−381.822
β_{xyz}	45.634
β_{yyz}	15.898
β_{xzz}	−49.332
β_{yzz}	−5.495
β_{zzz}	9.750
β_{tot}	13.834
Dipole moment	
μ_x	−1.0342
μ_y	1.9018
μ_z	0.5667
μ	5.192
Polarizability	
α_{xx}	352.666
α_{xy}	3.400
α_{yy}	170.081
α_{xz}	6.492
α_{yz}	−0.942
α_{zz}	72.318
α	29.396
HOMO – LUMO	
E_{HOMO}	−5.850
E_{LUMO}	−2.024
$E_{HOMO-LUMO}$	3.826
I	5.850
A	2.024
χ	3.937
η	1.913
S	0.261

of increase of potential is, red < orange < yellow < green < blue. The electrophiles tend to the negative and the nucleophiles tend to the region of positive ESP. In BDP, the carbonyl group behaves as electrophiles region and it is denoted as red color. Likewise, the nucleophiles region was graphically shown as blue color. Molecular surfaces obtained by B3LYP/6-31G(d,p) are shown in Fig. 9.

Table 6. Hyperpolarizability of BDP and some chalcones

Compound	β ($\times 10^{-30}$) (in esu)	Ref
BDP	13.834	Present work
1-(4-Aminophenyl)-3-(3,4-dimethoxyphenyl)-prop-2-en-1-one	24.8	[15]
(2E,6E)-2-(4-fluorobenzylidine)-6- (4-methoxybenzylidine) cyclohexanone	7.066	[16]
4-methoxy-4′-chlorochalcone	12.436	[17]
1,5-diphenylpenta-2,4-dien-1-one	7.077	[33]
1,5-diphenylpenta-1,4-dien-3-one	8.639	[34]
(2E,6E)-2-benzylidene-6-(4-methoxybenzylidene)cyclohexanone	3.414	[35]
4-Fluro chalcone	12.572	[36]

3.9. Mulliken Atomic Charges

In the application of quantum mechanical calculations to molecular systems, the calculation of effective atomic charge plays an important role. Mulliken atomic charges are calculated by determining the electron population of each atom as defined by the basis function. Fig. 10 shows the Mulliken atomic charges of BDP. The carbon atom C(10) has the highest positive (0.3880) charge when compared with all other ring carbon

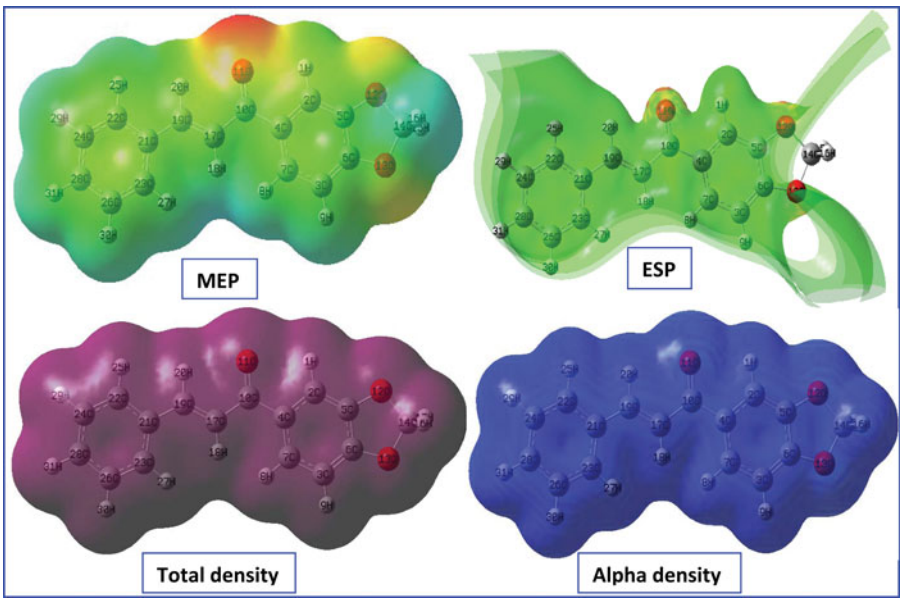

Figure 9. Molecular surface images of BDP.

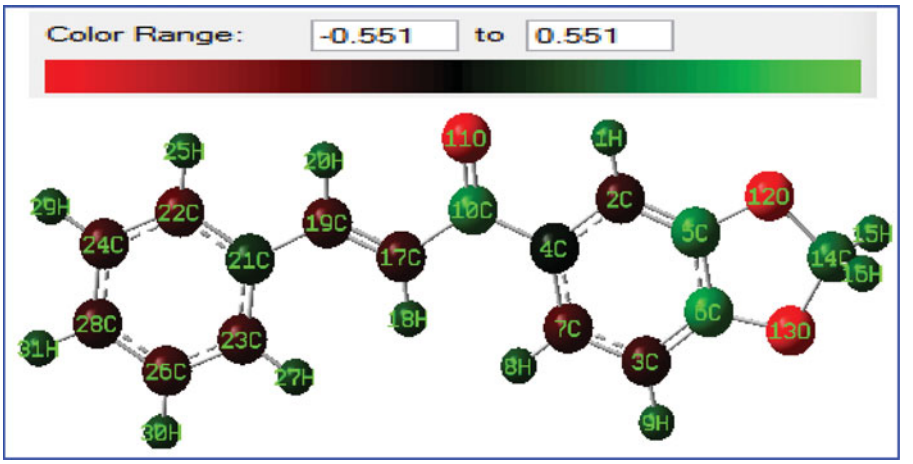

Figure 10. Mulliken atomic charge representation of BDP.

atoms (Fig. 10). From the listed tabulated values (Table 7) of atomic charge, the oxygen at O11, O12, and O13 in BDP has a large negative charge and behaved as electron donors and the rest of the atoms had positive charge and they are behaved as acceptor; suggest the presence of inter molecular hydrogen bonding interaction in the BDP molecule.

3.10. HOMO–LUMO energy

The highest occupied molecular orbital (HOMO) and lowest unoccupied molecular orbital (LUMO) of plots of BDP is shown in Fig. 11. The frontier orbital gap facilitates in characterizing the chemical reactivity and kinetic stability of the molecule. The red and green colors represent the positive and negative values for the wave function. The HOMO is the orbital that primarily acts as an electron donor and the LUMO is the orbital that mainly acts as an electron acceptor. The calculated HOMO–LUMO energy gap value is found to be 3.826 eV (Table 5).

HOMO and LUMO energies, the energy gap, ionization potential (I), electron affinity (A), electronegativity (χ), average hardness (η), and softness (S) of the BDP have been computed by B3LYP/6-31G(d,p) method and they are summarized in Table 5. By the computed value of HOMO and LUMO energy values for the BDP, the electronegativity, chemical hardness, and softness can be calculated as follows: $\chi = \frac{I+A}{2}$ (electronegativity), $\eta = \frac{I-A}{2}$ (chemical hardness), $S = 1/2\ \eta$ (chemical softness), where I ($-E_{HOMO}$) and A ($-E_{LUMO}$) are ionization potential and electron affinity respectively [37].

4. Conclusions

In this article, we have reported synthesis and characterization of a novel dioxolane ring containing organic crystal, 1-(benzo[d][1,3]dioxol-5-yl)-3-phenylprop-2-en-1-one. The product formation was confirmed by FT–IR and single-crystal XRD analyses. The powder X-ray

Table 7. Mulliken atomic charges of BDP.

Atom No.	Atoms	Atomic charge/e
1	H	0.12871
2	C	−0.13235
3	C	−0.13032
4	C	0.024465
5	C	0.314464
6	C	0.330383
7	C	−0.12872
8	H	0.093722
9	H	0.104837
10	C	0.388207
11	O	−0.49334
12	O	−0.53872
13	O	−0.53517
14	C	0.287749
15	H	0.126954
16	H	0.121913
17	C	−0.15609
18	H	0.089961
19	C	−0.09887
20	H	0.089631
21	C	0.118975
22	C	−0.07801
23	C	−0.11464
24	C	−0.12788
25	C	−0.08914
26	C	−0.09449
27	H	0.145266
28	H	0.084339
29	H	0.087528
30	H	0.09174
31	H	0.088911

diffraction study shows the good crystallinity of the material. Thermal stability was analyzed by TG/DTA study. Good transmission in the visible region is observed and the computed UV-vis spectrum shows that the excitations at 380, 369, and 318 nm, respectively. Theoretically calculated vibrational harmonic frequencies are compared with experimentally recorded spectrum. Molecular level nonlinearity with high first-order molecular hyperpolarizability is observed. The calculated HOMO and LUMO energies showed that charge transfer had occurred within the molecule. Molecular electrostatic potential map diagram shows that the negative potential sites are in electronegative atoms (denoted as red color) while the positive potential sites are around the hydrogen atoms (denoted as blue color).

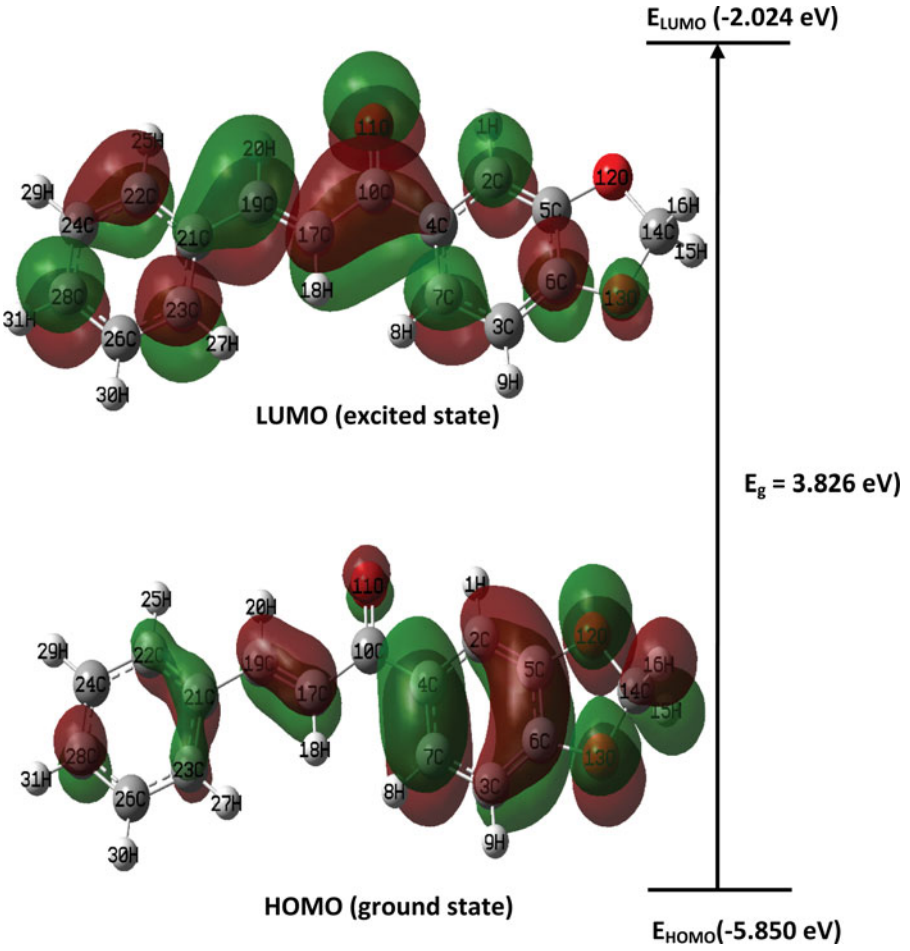

Figure 11. The frontier molecular orbital diagram of BDP.

Supplementary Material

CCDC 980067 contains the supplementary crystallographic data for this paper. These data can be obtained free of charge from The Cambridge Crystallographic Data Centre via www.ccdc.cam.ac.uk/data request/cif.

References

[1] Dimmock, J. R., Elias, D. W., Beazely, M. A., & Kandepu, N. M. (1999). *Curr. Med. Chem.*, *6*, 1125–1149.
[2] Shenvi, S., Krishna Kumar, Hatti, K. S., Rijesh, K., Latha Diwakar, & Chandrasekara Reddy, G. (2013). *Eur. J. Medi. Chem.*, *62*, 435–442.
[3] Opletalova, V. (2000). *Cesk. Farm.*, *49*, 278–284.
[4] Xia, Y., Yang, Z. Y., Xia, P., Bastow, G., Nakanishi, Y., & Lee, K. H. (2000). *Bioorg. Med. Chem. Lett.*, *10*, 699.
[5] Kumar, D., Maruthi Kumar, N., Akamatsu, K., Kusaka, E., Harada, H., & Ito, T. (2010). *Bioorg. Med. Chem. Lett.*, *20*, 3916–3919.
[6] Insuasty, B., Montoya, A., Becerra, D., Quiroga, J., Abonia, R., Robledo, S., Velez, I. D., Upegui, Y., Nogueras, M., & Justo Cobo. (2013). *Eur. J. Medi. Chem.*, *67*, 252–262.

[7] Popova, M., Bankova, V., Spassov, S., Tsvetkova, I., Naydenski, C., Silva, M. V., & Tsartsarova, M. (2001). *Z. Naturforsch. Teil C*, *56*, 593.
[8] Goto, Y., Hayashi, A., Kimura, Y., & Nakayam, M. (1991). *J. Cryst. Growth*, *108*, 688–698.
[9] Sarojini, B. K., Narayana, B., Ashalatha, B. V., Indira, J., & Lobo, K. G. (2000). *J. Cryst. Growth*, *295*, 54–59.
[10] Patil, P. S., Dharmaprakash, S. M., Hoong-Kun Fun, & Karthikeyan, M. S. (2006). *J. Cryst. Growth*, *297*, 111–116.
[11] Ravindra, H. J., Harrison, W. T. A., Suresh Kumar, M. R. & Dharmaprakash, S. M. (2009). *J. Cryst. Growth*, *311*, 310–315.
[12] John Kiran, A., Lee, H. W., Ravindra, H. J., Dharmaprakash, S. M., Kim, K., Lim, H., & Rotermund, F. (2010). *Curr. Appl. Phys.*, *10*, 1290–1296.
[13] Manjunath, H. R., Rajesh Kumar, P. C., Naveen, S., Ravindrachary, V., Sridhar, M. A., Prasad, J. S., & Karegoudar, P. (2011). *J. Cryst. Growth*, *327*, 161–166.
[14] Dsilva, E. D., Podagatlapalli, G. K., Venugopal Rao, S., & Dharmaprakash, S. M. (2012). *Opt. Laser Tech.*, *44*, 1689–1697.
[15] Joseph, L., Sajan, D., Shettigar, V., Chaitanya, K., Misra, N., Sundius, T., & Nemec, I. (2013). *Mater. Chem. Phys.*, *141*, 248–262.
[16] Meenatchi, V., Muthu, K., Rajasekar, M., & Meenakshisundaram, SP. (2013). *Physica B*, *419*, 95–99.
[17] Prabu, S., Nagalakshmi, R., Balaji, J., & Srinivasan, P. (2014). *Mater. Res. Bull.*, *50*, 446–453.
[18] Fichou, D., Watanabe, T., Takeda, T., Miyata, S., Goto, Y., & Nakayama, M. (1988). *Jpn. J. Appl. Phys*. *27*, L429.
[19] Uchida, T., Kozawa, K., Sakai, T., Aoki, M., Yoguchi, H., Abdureyam, A., & Watanebe, Y. (1998). *Mol. Cryst. Liq. Cryst.*, *315*, 135–140.
[20] Zhang, G., Kinoshita, T., Sasaki, K. Goto, Y., & Nakayam, M. (1990). *J. Cryst. Growth*, *100*, 411–416.
[21] Jayarama, A., Ravindra, H. J., Menezes, A. P., Dharmaprakash, S. M., & Weng Ng, S. (2013). *J. Mol. Struc.*, *1051*, 285–291.
[22] Bertl, E., Becker, H., Eicher, T., Herhaus, C., Kapadia, G., Bartsch, H., & Gerhauser, C. (2004). *Biochem. Biophys. Res. Commun.*, *325*, 287.
[23] Kitaoka, Y., Sasaki, T., Nakai, S., Yokotani, A., Goto, Y. & Nakayama, M. (1990). *Appl. Phys. Lett.*, *56*, 2074.
[24] Frisch, M. J., Trucks, G. W., & Schlegel, H. B. *et al.* (2009). *Gaussian-09, Revision C.01*, Gaussian Inc., Wallingford, CT.
[25] Schlegel, H. B. (1982). *J. Comput. Chem.*, *3*, 214–218.
[26] Frisch, A., Nielson, A. B., Holder, A. J., (2000). *Gaussview User Manual*, Gaussian Inc., Pittsburgh, PA.
[27] Kleinman, D. A. (1962). *Phys. Rev.*, *126*, 1977.
[28] Castiglioni, C., Del zoppo, M., Zuliani, P., & Zerbi, G. (1995). *Synth. Met.*, *74*, 171–177.
[29] Zuliani, P., Del zoppo, M., Castiglioni, C., Zerbi, G., Marder, S. R., & Perry, J. W. (1995). *Chem. Phys.*, *103*, 9935–9940.
[30] Del zoppo, M., Castiglioni, C. & Zerbi, G. (1995). *Non-Linear Opt*. *9*, 73.
[31] Del zoppo, M., Castiglioni, C., Zuliani, P., Razelli, A., Zerbi, G., & Blanchard-Desce, M. (1998). *J. Appl. Polym. Sci.*, *70*, 73.
[32] Ravikumar, C., Huber Joe, I., & Jayakumar, V. S. (2008). *Chem. Phys. Lett.*, *460*, 552–558.
[33] Rajasekar, M., Muthu, K. M., Bhagavannarayana, G., & Meenakshisundaram, S. P. (2012). *J. Appl. Cryst.*, *45*, 914–920.
[34] Sudha, S., Sundaraganesan, N., Vanchinathan, K., Muthu, K., & Meenakshisundaram, S. P. (2012). *J. Mol. Strut.*, *1030*, 191–203.
[35] Meenatchi, V., Muthu, K., Rajasekar, M., & Meenakshisundaram, S. P. (2014). *Spectrochim. Acta Part A*, *120*, 72–76.
[36] Prabu, S., Nagalakshmi, R., Balaji, J., & Srinivasan, P. (2014). *Spectrochim. Acta Part A*, *129*, 114–120.
[37] Pearson, R. G. (1986). *Proc. Natl. Acad. Sci.*, *83*, 8440–8441.